CHINESE OPTICS LETTERS

Vol. 19, No. 11 | November 2021

Simultaneous tailoring of longitudinal and transverse mode inside an Er:YAG laser

Rui Song (宋 睿)[1,2,3], Xueting Liu (刘雪婷)[1,2,3], Shiyao Fu (付时尧)[1,2,3*], and Chunqing Gao (高春清)[1,2,3**]

[1] School of Optics and Photonics, Beijing Institute of Technology, Beijing 100081, China

[2] Key Laboratory of Photoelectronic Imaging Technology and System, Ministry of Education, Beijing 100081, China

[3] Key Laboratory of Information Photonics Technology, Ministry of Industry and Information Technology, Beijing 100081, China

*Corresponding author: fushiyao@bit.edu.cn

**Corresponding author: gao@bit.edu.cn

Received March 30, 2021 | Accepted April 30, 2021 | Posted Online September 6, 2021

In this paper, we demonstrate a scheme to tailor both longitudinal and transverse modes inside a laser cavity and constitute an eye-safe single longitudinal mode $Er:Y_3Al_5O_{12}$ (Er:YAG) vector laser. A *q*-plate is employed as a spin-orbital conversion element to modulate the transverse mode and obtain cylindrical vector beams. An optical isolator is employed as a non-reciprocal element for the ring cavity to enforce unidirectional operation and achieve single longitudinal oscillation. The characteristics of power, transverse intensity, and polarization spectrum of the output beams are observed. The observed typical single longitudinal mode and highly matched special polarizations prove the successful tailoring of both longitudinal and transverse modes.

Keywords: Er:YAG; single longitudinal mode; cylindrical vector beam.

DOI: 10.3788/COL202119.111404

1. Introduction

Laser beams have a variety of physical dimensions like spatial structure, complex amplitude, polarization, time, wavelength/frequency, and so on. Generally, one can tailor one of them to obtain special beams including optical vortices[1], vector beams[2,3], ultrafast lasers[4], and single frequency lasers[5,6]. Beams located at ~1.6 μm operate in the eye-safe spectral range and are attractive for atmospheric applications such as wind-field velocity mapping[7] and atmospheric pollution monitoring[8]. Er^{3+}-doped media such as $Er:Y_3Al_5O_{12}$ (Er:YAG) are known for their ability to emit 1617 nm or 1645 nm with high efficiency and power scalability when they are band-pumped directly[9,10]. Lots of attentions have been paid recently to developing single frequency Er:YAG lasers. A ring cavity configuration with enforced unidirectional operation through a non-reciprocal element such as optical isolator (ISO) or traveling-wave acousto-optic modulator (AOM) could also produce 1.6 μm single frequency laser beams, and a 4.7 W single frequency Er:YAG ring laser with an AOM as a non-reciprocal element has been obtained[11].

Laser transverse mode tailoring usually refers to direct generation of complex structured beams inside the cavity, one of which is the beam with doughnut intensity patterns including scalar vortex beams carrying orbital angular momentum (OAM)[12,13] and cylindrical vector beams (CVBs) with inhomogeneous polarizations[14]. Such doughnut beams are also known as singular beams with phase or polarization singularity in the center and have already found lots of applications in optical tweezers[15], data transmission and processing[16], detection[17,18], and high-security encryption[19]. In recent years, many methods have been proposed for directly generating scalar vortices or CVBs from a laser cavity, such as off-axis pumping[20], spot-defect elements[21], annular pumping[22], inserting spin-orbital conversion elements[23], metamaterials[24], or electronically controlled liquid crystal devices[25]. However, most of the systems are 1 μm solid-state lasers with Nd^{3+}-doped media, and only a few have employed the above-mentioned methods in the eye-safe band. Among them, the method of annular pumping has been reported, and direct generation of radially polarized beams and scalar vortex pulses from Er:YAG lasers at 1.6 μm has been realized[26,27].

There are also a few studies that have tailored two or more of the laser beams' physical dimensions to enable the output laser to satisfy multiple applications at the same time. For instance, scalar vortex beams at 1 μm with a single longitudinal mode have been obtained through annual pumping in a short cavity and off-axis pumping in a non-planar ring oscillator (NPRO)[28,29]. In addition, a 1645 nm wavelength-tuning Er:YAG laser has been realized with annual pumping and a volume Bragg grating (VBG) as a folding mirror[30]. To the best of our knowledge,

direct generation of beams with single longitudinal mode and inhomogeneous polarization from Er:YAG lasers at 1645 nm is absent, and such lasers combining the characteristics of a single frequency laser and a vector laser may broaden potential applications like detection.

In this paper, we demonstrate an Er:YAG laser with simultaneous tailoring of longitudinal and transverse modes, from which CVBs with single longitudinal mode have been generated. q-plates (QPs) with $q = 1/2$ and $q = 3/2$ are inserted inside the cavity to tailor the transverse mode, and then obtain the first-order and third-order CVBs, respectively. An optical ISO is inserted inside the cavity for unidirectional operation so as to realize the tailoring of the longitudinal mode. The maximum power of the third-order CVBs with a single longitudinal mode is 240 mW, and the observed single longitudinal mode and measuring result of the relative weight of the mode show a satisfactory operation for simultaneous tailoring of both longitudinal and transverse modes.

2. Results and Discussions

An Er:YAG laser illustrated in Fig. 1 is proposed to accomplish the longitudinal and transverse mode modulation, and thus to produce CVBs with single longitudinal mode. The pump source is a fiber-coupled laser diode with an emitting wavelength of 1470 nm, corresponding to the $^4I_{15/2} \rightarrow {}^4I_{13/2}$ Er^{3+} absorption transition. The pump beam is collimated by a lens (L1) with a focal length of 30 mm and focused by another lens (L2) with a focal length of 125 mm. The gain medium is a $\Phi 4 \times 50$ mm Er:YAG ceramics rod with a doping concentration of 0.25% (atomic fraction). Such a low doping concentration is to alleviate energy transfer upconversion (ETU). Both sides of the ceramics rod are optically polished and anti-reflection coated for pump wavelength and lasing wavelength. The calculated pump spot radius at the center of the gain medium is about 425 μm.

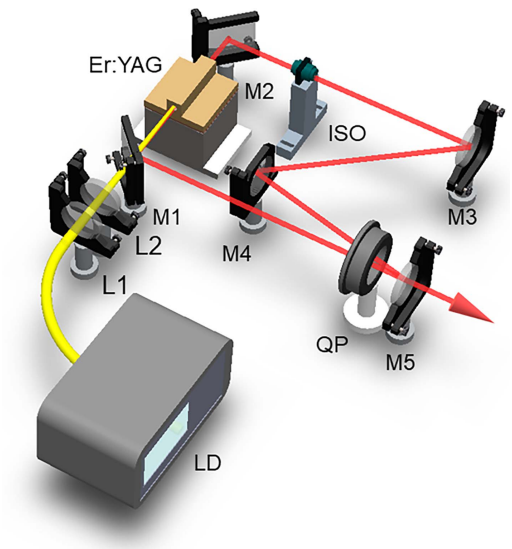

Fig. 1. Schematic diagram of the Er:YAG vector ring laser. LD, laser diode; L, lens; M1–M5, mirror; ISO, optical isolator; QP, q-plate. The incident angle at M5 drawn in the figure is much larger than that in the actual experiment for clear.

An M-shaped cavity containing five mirrors (M1–M5) is employed to constitute a ring cavity. M1 and M2 are used for the pump beam incidence and filtering out unabsorbed pump beams, respectively. Both of them are 45° dichroic mirrors coated with high-transmission coating at 1470 nm and high-reflection coating at 1645 nm. M3 is a folding mirror with a radius of curvature of 800 mm, coated for high reflectivity at 1645 nm. M4 is a flat mirror also coated for high reflectivity at 1645 nm. The output mirror M5 has a radius of curvature of 800 mm with a transmittance of 10% at 1645 nm. An optical ISO based on the Faraday effect is placed inside the cavity to achieve the unidirectional operation of the ring cavity laser. A QP is placed between the 45° dichroic mirror M1 and output mirror M5, which is as close as possible to M5. M4 is placed as close to M1 as possible here to make both the beam incident on M5 and the part of the beam reflected by M5 could be favorably modulated by the center of the QP. The incident angle of the beam at M5 is less than 2°.

For a stable oscillation, the polarization states and topological charges of the beam after each round trip in the cavity must return to the initial states, namely self-consistency. A QP is an inhomogeneous birefringent element, which can realize the spin-orbital interaction of photons[31]. The linearly polarized fundamental Gaussian beam turns to a CVB after passing through a QP. Previous works have already proved that a CVB generated by QP with q and an initial angle of α_0 can be decomposed into two orthogonal components as left and right-circular polarizations with opposite spiral phases:

$$\Phi_1 \exp(-i2\alpha_0)|-2q\rangle|R\rangle + \Phi_2 \exp(i2\alpha_0)|2q\rangle|L\rangle, \quad (1)$$

where Φ_1 and Φ_2 are complex coefficients, and they are equal for horizontally polarized beams. After being reflected by the output mirror M5, the circular polarization rotation and topological charges of each component are all opposite:

$$\Phi_1 \exp(-i2\alpha_0)|2q\rangle|L\rangle + \Phi_2 \exp(i2\alpha_0)|-2q\rangle|R\rangle. \quad (2)$$

After passing through the QP again, the reflected beam of M5 becomes the same as that incident on the QP for the first time. Thus, self-consistency of the mode is realized. In essence, only the beam transmitted between QP and the output mirror M5 is a CVB and, in the other parts, is a fundamental Gaussian beam, which greatly enhances the stability of the laser.

Unidirectional and bidirectional operations are investigated with and without placing the ISO and QP to show the performance of longitudinal and transverse modulations. In the bidirectional operation, we firstly remove the QP, and no longitudinal or transverse modulations are introduced inside the cavity. The maximum output power is 5.79 W, and the corresponding slope efficiency is 31.6%.

After inserting a QP into the cavity, stable transverse mode modulation is realized. By now, the output beam changes from

a fundamental mode to a CVB. The polarization topological charge of the obtained CVB is determined by the q-value of the QP. Here, we use two QPs fabricated from polymerized liquid crystals, with q-values of 1/2 and 3/2, respectively. CVBs with the polarization topological charge of $p = 1$ and $p = 3$ are generated, respectively, and the main axes of the QPs are zeros, as arranged here. The input-output dependence for them is shown in Fig. 2. With the increase of pump power, CVB begins to appear for $p = 1$ and $p = 3$ above an incident pump power of 31 W and 33 W, respectively. The output power reaches 1.05 W and 0.71 W for $p = 1$ and $p = 3$, corresponding to a slope efficiency of 10.6% and 8.9%, respectively. Such a decrease in slope efficiency is due to insertion loss and mode conversion loss.

Figure 3(a) presents the intensity profiles captured by an infrared camera (Xenics, Bobcat-320-star, resolution 320 × 256 pixels). For comparison, the output fundamental Gaussian beams without inserting a QP are also recorded. Typical doughnut profiles of CVBs with $p = 1$ and $p = 3$ can be observed clearly with bidirectional outputs. Due to a much smaller incident angle at M5, the observed bidirectional output beams are close to each other, but one with better emission perpendicularity and better coincidence relative to the center of the QP obtains a better spot profile than the other one. We choose the better one to test the effect of transverse mode modulation, including polarization distribution and polarization topological charge. A polarization beam splitter (PBS) is placed between M5 and the camera, and the intensity profiles of the reflected part of CVBs with $p = 1$ and $p = 3$ are shown in Fig. 3(b). After that, a quarter-wave plate (QWP) with a fast axial angle of 45° is placed between M5 and the PBS to convert CVBs to multiplexed scalar vortex beams containing two components with orthogonal linear polarization states and opposite topological charges, which could be separated by the PBS. Both of the components pass through a tilted lens, respectively, and the far-field intensity profiles are observed and recorded again, as shown in Fig. 3(c). By counting the number and arranged orientation of bright stripes, one could determine their topological charges[32]. The results indicate the expected conversion of CVBs with $p = 1$ and $p = 3$ from fundamental Gaussian beams.

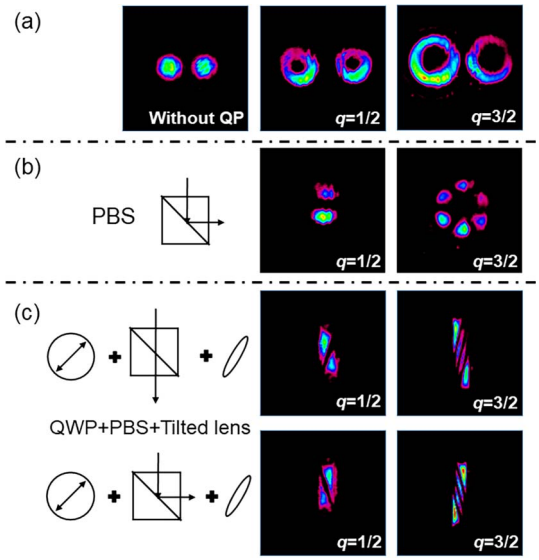

Fig. 3. (a) Doughnut profiles of fundamental Gaussian beams and CVBs with p = 1 and p = 3; (b) intensity distributions after passing through a PBS; (c) observed intensity distributions after passing through a tilted lens.

Next, an optical ISO is placed into the cavity to realize unidirectional operation, thereby eliminating the spatial-hole-burning effect. Both transverse and longitudinal modes distributions in the cavity could be modulated, and CVBs with a single longitudinal mode are obtained. As displayed in Fig. 4, for CVBs with $p = 1$ and $p = 3$, the maximum output power is 488 mW and 240 mW at the highest incident pump power, respectively.

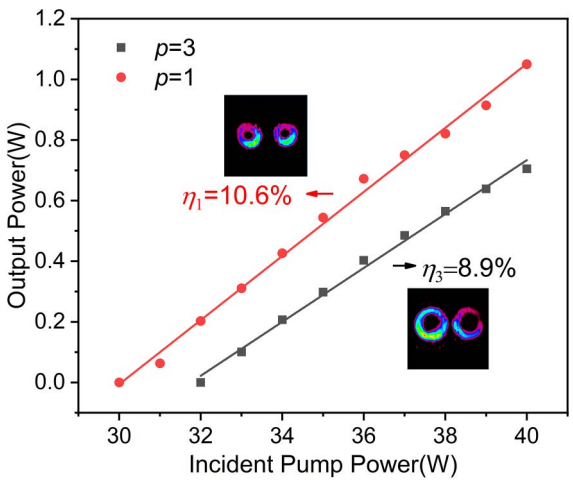

Fig. 2. Input-output dependences of CVBs with p = 1 and p = 3 in bidirectional operation.

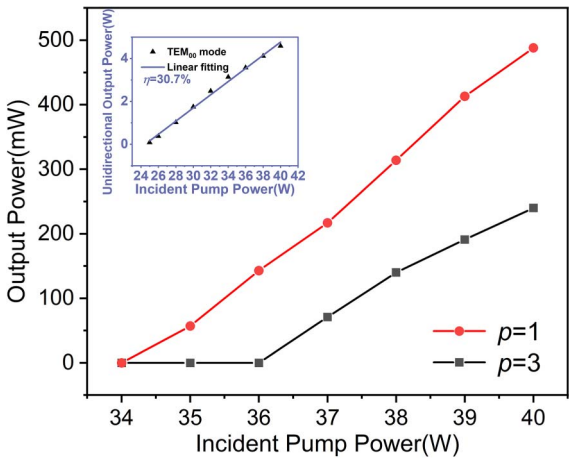

Fig. 4. Input-output dependences of CVBs with p = 1 and p = 3 in unidirectional operation. Inset: input-output dependences of the fundamental Gaussian beam in unidirectional operation.

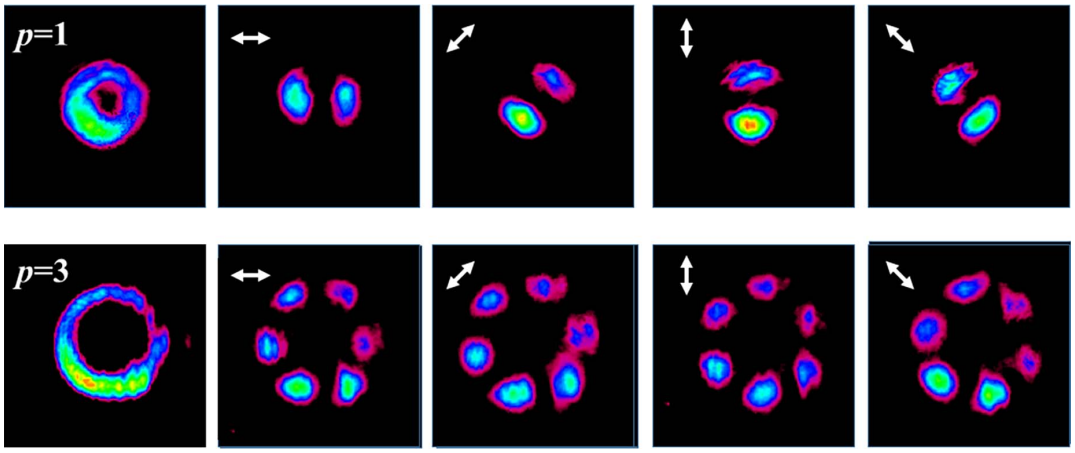

Fig. 5. Doughnut profiles of CVBs with $p = 1$ and $p = 3$ in unidirectional operation and the corresponding intensity distributions after passing through an analyzer with different axis angles.

Figure 5 shows the intensity patterns of output CVBs in a unidirectional operation and their corresponding intensity distributions after passing through an analyzer with various axis angles. Obviously, lobe-like patterns are present, and such lobes rotate with the rotation of the analyzer axis, which highly matches special polarization distributions of the CVBs. The single longitudinal output performance is also evaluated through a scanning Fabry–Perot (F–P) interferometer. Figure 6 gives the scanning spectrum of the generated CVB ($p = 3$) in unidirectional and bidirectional operation, respectively. Figure 6(b) shows the typical single longitudinal mode lasing signal, indicating a single longitudinal CVB is well generated.

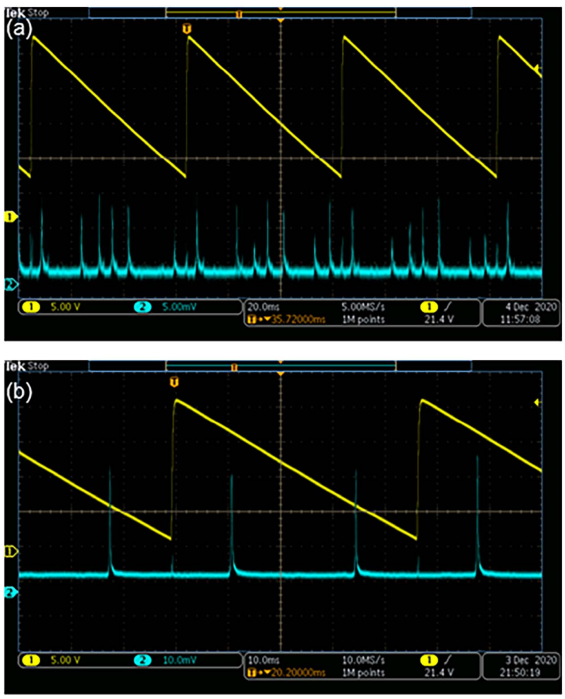

Fig. 6. Scanning spectra of the output CVB ($p = 3$) in (a) bidirectional operation and (b) unidirectional operation.

We also evaluate the OAM distribution of the produced single weight CVBs, taking $p = 3$ for instance. Figure 7(a) shows the schematic diagram for relative weight measurement of CVBs with a single longitudinal mode. The CVB emitted from the cavity is incident in a PBS, and the transmitted part is a horizontal linearly polarized OAM beam with topological changes of ±3. Note that a PBS is used here because the liquid crystal spatial light modulator (SLM) (Holoeye, PLUTO-TELCO-013-C) we use only introduces the phase-only modulation for horizontal linear polarizations. The holograms of the spiral phase plates (SPPs) with the topological charges of −10 to +10 are encoded on the SLM in sequence, thus to back-convert the modes. The modulated beams are then focused by a lens, and the back-converted patterns in the far field are recorded as grayscale images by the infrared camera. The OAM spectrum could be obtained from analyzing and calculating those images by the grayscale algorithm[33]. One could see that the relative weight of the single longitudinal mode CVB with $p = 3$ is high enough, as described in Fig. 7(b).

We have demonstrated an Er:YAG single longitudinal mode vector laser based on QPs and optical ISOs and showed the output power, spot profile, polarization, relative mode weight, and spectrum. Here, we use QPs with $q = 1/2$ and $q = 3/2$ to get CVBs with $p = 1$ and $p = 3$. Changing other q-value QPs could achieve higher-order CVBs. Besides, by rotating the QPs, CVBs with other polarization distributions could also be obtained. In addition, due to the mechanical assembly of QPs and rotation mount used here, there is a certain distance between the QP and the output mirror, which prevents them from being completely close. Therefore, conversion losses are introduced and, thus, deflects the profile of the output beam. By optimizing the assembly method or the design of the cavity, the distance between the QP and the output mirror could be shortened, so that the incident points of the incident beam and reflected beam of M5 at the QP would have a better coincidence.

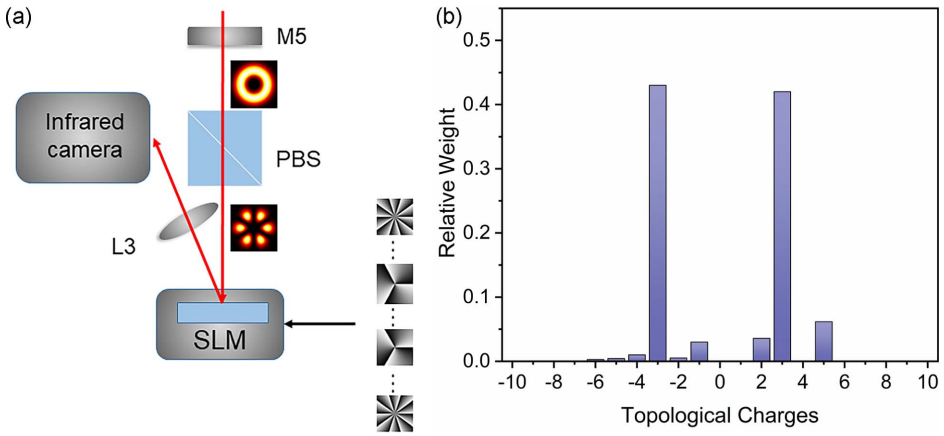

Fig. 7. (a) Schematic diagram for measuring the relative OAM weight of generated beams; (b) the measured OAM weight distribution through the SPP embedded back-converted method.

3. Conclusion

In summary, a 1645 nm Er:YAG vector laser with simultaneous tailoring of longitudinal and transverse modes has been realized. An optical ISO and a QP are employed as a non-reciprocal element and a photon spin-orbital conversion element to tailor longitudinal and transverse modes inside the laser resonator, respectively. The beam output power and profiles of bidirectional output and unidirectional output including fundamental Gaussian beam and CVBs with $p = 1$ and $p = 3$ are measured and analyzed. The topological charges are investigated through a tilted lens, and the performance of single longitudinal mode oscillation is verified by an F–P scanning interferometer. Furthermore, we also measured the relative weight of the generated single longitudinal mode CVBs. We believe that such an Er:YAG vector laser with a single longitudinal mode can inspire lots of applications in the fields of remote sensing, communication, and spectroscopy.

Acknowledgement

This work was supported by the National Key Research and Development Program of China (No. 2017YFB0405203), National Natural Science Foundation of China (Nos. 11834001 and 61905012), and National Defense Basic Scientific Research Program of China (No. JCKY2020602C007).

References

1. X. Huang, B. Xu, S. Cui, H. Xu, Z. Cai, and L. Chen, "Direct generation of vortex laser by rotating induced off-axis pumping," IEEE J. Sel. Top. Quantum Electron. **24**, 1601606 (2018).
2. S. Iwahashi, Y. Kurosaka, K. Sakai, K. Kitamura, N. Takayama, and S. Noda, "Higher-order vector beams produced by photonic-crystal lasers," Opt. Express **19**, 11963 (2011).
3. S. Chen, J. Li, and K.-I. Ueda, "Cylindrical vector beam rotary Nd:YAG disk laser with birefringent crystal," Chin. Opt. Lett. **18**, 121401 (2020).
4. Z.-X. Ding, Z.-N. Huang, Y. Chen, C. Mou, Y.-Q. Lu, and F. Xu, "All-fiber ultrafast laser generating gigahertz-rate pulses based on a hybrid plasmonic microfiber resonator," Adv. Photon. **2**, 026002 (2020).
5. X. Cao, P. Li, and Q. Liu, "Theoretical and experimental investigation of injection seeded Nd:YAG zigzag slab ring lasers," Opt. Laser Technol. **123**, 105912 (2020).
6. Y. Zhang, C. Gao, Q. Wang, Q. Na, M. Zhang, M. Gao, and S. Huang, "1 kHz single-frequency, injection-seeded Er:YAG laser with an optical feedback," Chin. Opt. Lett. **17**, 031402 (2019).
7. K. Wang, C. Gao, Z. Lin, Q. Wang, M. Gao, S. Huang, and C. Chen, "1645 nm coherent Doppler wind lidar with a single-frequency Er:YAG laser," Opt. Express **28**, 14694 (2020).
8. C. Stephan, M. Alpers, B. Millet, G. Ehret, P. Flamant, and C. Deniel, "MERLIN–a space-based methane monitor," Proc. SPIE **8159**, 815908 (2011).
9. J. O. White, M. Dubinskii, L. D. Merkle, I. Kudryashov, and D. Garbuzov, "Resonant pumping and upconversion in 1.6 μm Er^{3+} lasers," J. Opt. Soc. Am. B **24**, 2454 (2007).
10. S. Li, Q. Wang, R. Song, F. Hou, M. Gao, and C. Gao, "Laser diode pumped high-energy single-frequency Er:YAG laser with hundreds of nanoseconds pulse duration," Chin. Opt. Lett. **18**, 031401 (2020).
11. J. W. Kim, J. K. Sahu, and W. A. Clarkson, "Efficient single-axial-mode operation of an Er:YAG ring laser at 1645 nm," in *Conference on Lasers and Electro-Optics/Quantum Electronics and Laser Science Conference and Photonic Applications Systems Technologies* (Optical Society of America, 2008), paper CTuAA4.
12. L. Allen, M. W. Beijersbergen, R. J. C. Spreeuw, and J. P. Woerdman, "Orbital angular momentum of light and the transformation of Laguerre–Gaussian laser modes," Phys. Rev. A **45**, 8185 (1992).
13. A. M. Yao and M. J. Padgett, "Orbital angular momentum: origins, behavior and applications," Adv. Opt. Photon. **3**, 161 (2011).
14. Q. Zhan, "Cylindrical vector beams: from mathematical concepts to applications," Adv. Opt. Photon. **1**, 1 (2009).
15. M. Padgett and R. Bowman, "Tweezers with a twist," Nat. Photon. **5**, 343 (2011).
16. J. Wang, J.-Y. Yang, I. M. Fazal, N. Ahmed, Y. Yan, H. Huang, Y. Ren, Y. Yue, S. Dolinar, M. Tur, and A. E. Willner, "Terabit free-space data transmission employing orbital angular momentum multiplexing," Nat. Photon. **6**, 488 (2012).
17. M. P. J. Lavery, F. C. Speirits, S. M. Barnett, and M. J. Padgett, "Detection of a spinning object using light's orbital angular momentum," Science **341**, 537 (2013).
18. S. Fu, T. Wang, Z. Zhang, Y. Zhai, and C. Gao, "Non-diffractive Bessel–Gauss beams for the detection of rotating object free of obstructions," Opt. Express **25**, 20098 (2017).
19. X. Fang, H. Ren, and M. Gu, "Orbital angular momentum holography for high-security encryption," Nat. Photon. **14**, 102 (2020).
20. S. Cui, N. Li, B. Xu, H. Xu, Z. Cai, J. Pu, and S. Chávez-Cerda, "Direct generation of visible vortex Hermite–Gaussian modes in a diode-pumped Pr:YLF laser," Opt. Laser Technol. **131**, 106389 (2020).

21. Z. Qiao, G. Xie, Y. Wu, P. Yuan, J. Ma, L. Qian, and D. Fan, "Generating high-charge optical vortices directly from laser up to 288th order," Laser Photon. Rev. **12**, 1800019 (2018).
22. T. Sato, Y. Kozawa, and S. Sato, "Transverse-mode selective laser operation by unicursal fast-scanning pumping," Opt. Lett. **40**, 3245 (2015).
23. D. Naidoo, F. S. Roux, A. Dudley, I. Litvin, B. Piccirillo, L. Marrucci, and A. Forbes, "Controlled generation of higher-order Poincaré sphere beams from a laser," Nat. Photon. **10**, 327 (2016).
24. H. Sroor, Y.-W. Huang, B. Sephton, D. Naidoo, A. Vallés, V. Ginis, C.-W. Qiu, A. Ambrosio, F. Capasso, and A. Forbes, "High-purity orbital angular momentum states from a visible metasurface laser," Nat. Photon. **14**, 498 (2020).
25. Y. Yang, Q. Zhao, L. Liu, Y. Liu, C. Rosales-Guzmán, and C.-W. Qiu, "Manipulation of orbital-angular-momentum spectrum using pinhole plates," Phys. Rev. Appl. **12**, 064007 (2019).
26. J. W. Kim, J. I. Mackenzie, J. R. Hayes, and W. A. Clarkson, "High power Er:YAG laser with radially-polarized Laguerre–Gaussian (LG_{01}) mode output," Opt. Express **19**, 14526 (2011).
27. Y. Zhao, Q. Liu, W. Zhou, and D. Shen, "~1 mJ pulsed vortex laser at 1645 nm with well-defined helicity," Opt. Express **24**, 15596 (2016).
28. D. J. Kim and J. W. Kim, "Direct generation of an optical vortex beam in a single-frequency Nd:YVO_4 laser," Opt. Lett. **40**, 399 (2015).
29. G. Lin, Y. Cao, R. Ji, C. Hou, and Z. Lu, "Direct generation of a narrow-linewidth Laguerre–Gaussian vortex laser in a monolithic nonplanar oscillator," Opt. Lett. **43**, 4164 (2018).
30. Q. Liu, Y. Zhao, M. Ding, W. Yao, X. Fan, and D. Shen, "Wavelength- and OAM-tunable vortex laser with a reflective volume Bragg grating," Opt. Express **25**, 23312 (2017).
31. A. Rubano, F. Cardano, B. Piccirillo, and L. Marrucci, "Q-plate technology: a progress review [Invited]," J. Opt. Soc. Am. B **36**, D70 (2019).
32. P. Vaity, J. Banerji, and R. P. Singh, "Measuring the topological charge of an optical vortex by using a tilted convex lens," Phys. Lett. A **377**, 1154 (2013).
33. S. Fu, S. Zhang, T. Wang, and C. Gao, "Measurement of orbital angular momentum spectra of multiplexing optical vortices," Opt. Express **24**, 6240 (2016).